Published in final edited form as:
Cancer Res. 2010 December 1; 70(23): 9855–9864. doi:10.1158/0008-5472.CAN-10-0250.

Photothermal Response of Human and Murine Cancer Cells to Multiwalled Carbon Nanotubes after Laser Irradiation

Jessica W. Fisher[1], **Saugata Sarkar**[2], **Cara F. Buchanan**[1], **Christopher S. Szot**[1], **Jon Whitney**[2], **Heather C. Hatcher**[3], **Suzy V. Torti**[4], **Christopher G. Rylander**[1,2], and **Marissa Nichole Rylander**[1,2]

[1]School of Biomedical Engineering and Sciences, Virginia Tech, Blacksburg, Virginia

[2]Department of Mechanical Engineering, Virginia Tech, Blacksburg, Virginia

[3]Department of Cancer Biology, Wake Forest University School of Medicine, Winston-Salem, North Carolina

[4]Department of Biochemistry and the Comprehensive Cancer Center, Wake Forest University School of Medicine, Winston-Salem, North Carolina

Abstract

This study demonstrates the capability of multiwalled carbon nanotubes (MWNTs) coupled with laser irradiation to enhance treatment of cancer cells through enhanced and more controlled thermal deposition, increased tumor injury, and diminished heat shock protein (HSP) expression. We also explored the potential promise of MWNTs as drug delivery agents by observing the degree of intracellular uptake of these nanoparticles. To determine the heat generation capability of MWNTs, the absorption spectra and temperature rise during heating were measured. Higher optical absorption was observed for MWNTs in water compared with water alone. For identical laser parameters, MWNT-containing samples produced a significantly greater temperature elevation compared to samples treated with laser alone. Human prostate cancer (PC3) and murine renal carcinoma (RENCA) cells were irradiated with a 1,064-nm laser with an irradiance of 15.3 W/cm^2 for 2 heating durations (1.5 and 5 minutes) alone or in combination with MWNT inclusion. Cytotoxicity and HSP expression following laser heating was used to determine the efficacy of laser treatment alone or in combination with MWNTs. No toxicity was observed for MWNTs alone. Inclusion of MWNTs dramatically decreased cell viability and HSP expression when combined with laser irradiation. MWNT cell internalization was measured using fluorescence and transmission electron microscopy following incubation of MWNTs with cells. With increasing incubation duration, a greater number of MWNTs were observed in cellular vacuoles and nuclei. These findings offer an initial proof of concept for the application of MWNTs in cancer therapy.

Introduction

In the United States, it is estimated that more than 1.52 million people will receive a diagnosis of cancer and more than 569,000 people will die of this disease in 2010 (1). Minimally invasive thermal therapies are being investigated such as laser-based photothermal therapy (2–4), microwave and radio-frequency ablation (5, 6), magnetic

Corresponding Author: Marissa Nichole Rylander; ICTAS Building, Stanger Street, Blacksburg, VA 24061. Phone: 540-231-3134; Fax: 540-231-0970; mnr@vt.edu.

Disclosure of Potential Conflicts of Interest
No potential conflicts of interest were disclosed.

thermal ablation (7, 8), and focused ultrasonography (9). However, the effectiveness of such treatments is limited by nonspecific heating of target tissue, often leading to healthy tissue injury. In addition, thermal therapies can frequently be compromised because of induction of molecular chaperones, known as heat shock proteins (HSPs), in regions of the tumor where nonlethal thermal dose exists (insufficient temperature elevation or heating duration) (10, 11). HSPs are a diverse family of stress-inducible chaperone proteins involved in protein refolding, trafficking, and antiapoptotic signaling (11–18). Elevated temperatures typically above the threshold of 43°C cause significant induction of HSPs, thereby permitting HSPs to serve as endogenous cellular markers of thermal stress. Thermal induction of HSPs can lead to increased tumor recurrence by enhancing tumor cell viability and imparting resistance to subsequent chemotherapy and radiation treatments (10–13, 17–20). Therefore, measurement of HSPs following thermally based therapies can indicate significant yet sublethal temperature elevation, delineate tumor regions with a high likelihood of treatment failure, and permit evaluation of the efficacy of applied thermal therapies. Specifically, induction of HSPs (HSP27, HSP70, and HSP90; number denotes molecular weight in kilodaltons) can serve as thermal therapy outcome predictors due to their role in cancer progression (11, 13, 18, 19) and characterized thermally induced kinetics (21–25).

To enhance thermal deposition and heating selectivity of photothermal therapies, researchers have explored the potential of nanoparticles as heat delivery vehicles for laser treatment of tumors (26–31). We are investigating MWNTs because their electrical antenna properties are far superior to single-walled nanotubes (SWNTs) and nanoshells, with their absorption being higher than that of other nanoparticles (26, 31). According to classic antenna theory, optical coupling of light and nanotubes is predicted to be most efficient for nanotube lengths that are at least half the wavelength of the These wavelengths allow the nanotube to become an electrical dipole for incident radiation (32, 33). Because the currents within the particle have significantly long dephasing times, traveling essentially without scatter (ballistically on/within the tube), the nanotube is a “super-antenna,” as reported by others (34, 35). MWNTs can absorb approximately 3 times the amount of light as SWNTs per particle and behave as highly efficient dipole antennae with broad absorption spectra compared with the specific resonance absorptions of SWNTs and nanoshells, which is critical due to light attenuation and scattering in skin and subcutaneous tissue. MWNTs can be expected to absorb significantly more near-infrared (NIR) radiation than SWNTs both because MWNTs have more available electrons for absorption per particle and possess greater mass. This comparison of SWNTs and MWNTs has been shown in previous research (36, 37). Because of the absence of NIR absorbing chromophores, NIR light can penetrate skin with minimal heating (29, 30). Previous work has shown that MWNTs coupled with NIR light can generate heat with remarkable efficiency, producing lethal temperatures (36, 37). Therefore, introducing MWNTs within the target tissue can greatly enhance heat diffusion, increasing the amount and specificity of thermal deposition.

Minimal information has been published regarding cellular response in terms of thermal injury, HSP expression, and intracellular transport of MWNTs alone or in combination with laser treatment. Furthermore, determination of optimal laser parameters and MWNT properties is necessary for developing effective therapies capable of maximizing temperature elevation and thermal injury to mitigate HSP expression within the target tumor volume.

This study investigated whether incorporating MWNTs into laser treatment of cancer cells could increase heat deposition for enhanced tumor cell destruction and downregulation of HSP expression. We also explored the capability of MWNTs for intracellular uptake for future use in thermally mediated drug delivery. The thermal enhancing ability of MWNTs was confirmed through absorption, heat generation, cell viability, and HSP expression

measurements. Our results show no inherent toxicity of MWNTs when incorporated within cells. When appropriate laser parameters were used in combination with MWNT inclusion, significant temperature elevations, decreased cell viability, and downregulation of HSP expression can be achieved, leading to a successful cancer treatment alternative. Significant levels of MWNT cellular uptake confirmed the possibility of their use in imaging, drug delivery, and multimodal therapies.

Materials and Methods

Cells

To determine the effectiveness of MWNTs in combination with laser therapy for enhancing photothermal mediated cancer cell death, we investigated the response of 2 different types of cancer cell lines. A human androgen-independent prostate cancer cell line (PC3) was purchased from American Type Culture Collection (ATCC® CRL-1435™) and was cultured in RPMI 1640 media with L-glutamine (Mediatech) and supplemented with 10% fetal bovine serum and 1% Pen-Strep (Sigma-Aldrich). A murine renal cancer cell line (RENCA) was obtained in July 2007 at passage 3 following an *in vivo* passage in mice and was a generous gift of Dr. R. Wiltrout (NCI Frederick). These cells were cultured for a maximum of 8 weeks before use and were not reauthenticated. The culture media was the same formulation as PC3 media except for the addition of 1% sodium pyruvate (Mediatech). Cell cultures were maintained in a 5% CO_2 incubator at 37°C in T25 (25-cm^2 area) flasks. For all experiments, cell monolayers were grown on coated 2-chamber glass slides (Fisher Scientific) at a density of 100,000 cells per chamber and seeded 24 hours before experimentation. During laser heating, culture media was removed and sterile-filtered Eagle's minimum essential medium (Sigma-Aldrich) was mixed with MWNTs and used during heating. Using this media prevented thermally induced media protein coagulation during the laser heating process, which can be toxic to cells.

Functionalization of MWNTs

MWNTs (length: 900 nm) were fabricated by chemical vapor deposition at Wake Forest University by Dr. David Carroll's group, as described previously (36, 38). Previous studies have shown that the absorption and heat generation by MWNTs following photoexcitation are a function of length (32, 33, 36). Although all MWNTs absorb light, MWNTs with lengths greater than 900 nm exhibit the greatest absorption at 1,064 nm according to electrical antenna theory (32, 33, 36, 37, 39). MWNTs were suspended in deionized water with 1% Pluronic F-127 (PL-127) by sonication and sterilized in a steam autoclave. PL-127 permitted the creation of a monodisperse MWNT solution, with Pluronic at a concentration of 1% in water was used based on its biocompatibility and proven dispersion abilities of nanotubes (36, 37, 40, 41). A 0.1 mg/mL of MWNT solution was used for all experiments, based on previous measurements demonstrating effective heating at this concentration (36, 37).

Optical absorption

Optical absorption of water with and without MWNT inclusion was measured with a double-beam Cary 5000 spectrophotometer (Varian, Inc.) coupled with a DRA-2500 diffuse reflectance accessory (DRA) in a wavelength range of 200 to 1,800 nm. The absorbance of air was measured across this wavelength range and set as a zero baseline for comparison with MWNT solutions and deionized water. MWNT solution and water samples were placed in quartz cuvettes (Starna Cells) within the DRA and absorbance was measured and analyzed.

Temperature measurement

Samples with and without MWNT inclusion were laser irradiated by a continuous wave, ytterbium fiber laser, YLD-5-1064-LP (IPG Photonics), with an irradiance of 15.3 W/cm^2 [3 W, 5-mm beam diameter (spot size)] at 1,064-nm wavelength for heating durations of 1.5 and 5 minutes. Cells were not individually targeted, but the MWNTs were responsible for raising the bulk extracellular media temperature. This irradiance was used for the majority of experiments involving the measurement of photothermal response (temperature, cell viability, and HSP expression). Therefore, this value will frequently not be specified subsequently in this article but can be assumed unless otherwise designated. To determine the equivalent heating dose to cause comparable cell death without MWNTs, several samples were also laser heated with the same irradiance but with a heating duration of 10 minutes. Samples were also exposed to a higher irradiance of 50.9 W/cm^2 [10 W, 5-mm beam diameter (spot size)] for durations of 5 and 10 minutes. Two hypodermic thermocouples were placed in the media of the culture chamber at known distances (4 and 7 mm from the laser center) to measure real-time temperature elevations. A National Instruments thermocouple reader (USB-9211) and VI Logger Lite software was used to record temperature data during the experiments.

Cell viability

Cell viability was measured for samples exposed to MWNTs or laser irradiation (15.3 W/cm^2 for 1.5 or 5 minutes) alone or in combination. Cells were stained with trypan blue, a membrane permeability dye that permeates only dead or dying cells due to compromised membrane integrity (dead cells appear blue because of dye uptake). PC3 and RENCA cells were seeded for 24 hours and then incubated with MWNTs for 16, 24, and 48 hours. The cell viability was measured for samples with MWNT inclusion alone (−Laser, +NT) and compared with samples without MWNTs (−Laser, −NT), which signified their native state. The ability of MWNTs to enhance tumor cell death when coupled with laser irradiation was also determined by comparing the measured cell viability for cells exposed to only laser heating (+Laser, −NT) to cells experiencing laser heating in combination with MWNT inclusion (+Laser, +NT). Cell viability of laser-treated samples was assessed at 16 hours post-heating with trypan blue staining to correspond with HSP expression measurements. For these experiments, sterile-filtered 0.4% trypan blue solution (Sigma-Aldrich) was diluted in warmed PBS (ratio 1:1). Culture media was removed and samples were rinsed with warmed PBS twice. Diluted trypan blue solution was added to samples for 5 minutes at room temperature, removed, and were rinsed with PBS twice and remained in PBS during imaging. A Leica inverted DMI6000B microscope was used to capture cell viability images. Within the field of view, the total number of cells and the number of unstained cells were counted. Cell viability was taken as the ratio of the number of unstained cells to total cells, with at least 3 samples for each heating regime.

HSP expression

Fluorescent immunostaining and image processing were used to visualize and quantify the expression of HSP27, HSP70, and HSP90 in untreated and laser-irradiated (15.3 W/cm^2 for 1.5 or 5 minutes) cell samples with and without MWNTs. HSP expression was measured at 16 hours post heating which has been shown to be the peak time for thermally induced HSP expression (21, 36, 37, 42). All incubation steps were carried out in the 37°C incubator (5% CO_2). Cells were rinsed with warmed PBS, fixed with Histochoice fixative MB (Electron Microscopy Sciences) for 20 minutes, rinsed, and permeabilized by 0.5% Triton X-100 (diluted in deionized water) to allow antibody staining. Cells were rinsed and incubated with a blocking buffer consisting of 5% normal goat sera (Santa Cruz Biotechnology, Inc.) diluted in PBS at 37°C for 1 hour. A primary antibody for HSP27 (SPA-800BD; dilution: 1:100), HSP70 (SPA-812C; dilution: 1:500), or HSP90 (SPA-835D; dilution: 1:100) from

Assay Designs was diluted in 1.5% normal goat sera and incubated with samples at 37°C for 1 hour. The fluorescent secondary antibodies Cyanine2 (for HSP27; dilution: 1:300; 016-220-084), AMCA (for HSP70; dilution: 1:50; 111–155–144), or Rhodamine Red-X (RRX; for HSP90; dilution: 1:50; 112–295–167) from Jackson Immunoresearch, were first diluted in deionized water and further diluted in PBS. After samples were rinsed to remove residual unbound primary antibodies, each secondary antibody was incubated with its corresponding sample at 37°C for 1 hour. Slides were rinsed, mounting media was applied, and cover slips were sealed before imaging. Samples were imaged using a Leica inverted DMI6000B microscope. Photoshop Elements 6.0 was used to assess average fluorescence intensity corresponding to HSP expression for each sample, analyzing a histogram of the fluorescence intensity of multiple regions of interest of a predetermined size (encompassing approximately 1–2 cells) within each sample. Mean fluorescence intensity and standard deviation were determined within these regions for each sample, with at least 3 samples being evaluated for each HSP of interest.

MWNT cellular uptake analysis

To explore the potential of MWNTs as intracellular transport vehicles for enhanced thermal therapy or drug delivery, the presence of MWNT internalization and distribution in cancer cells was captured using fluorescence imaging of DAPI-stained nuclei and transmission electron microscopy (TEM). For fluorescent visualization, RENCA and PC3 cells were seeded for 24 hours in 24-well plates and incubated with MWNTs for 24 hours. Cells were rinsed with warmed PBS to remove any surface-attached or free MWNTs in solution, fixed with Histochoice MB fixative (Electron Microscopy Sciences) for 20 minutes, rinsed 3 times, permeabilized with 0.5% Triton X-100, and rinsed 3 times again. Mounting media with DAPI (Vector Labs, Inc.) was incubated with samples for 10 minutes. A Leica inverted DMI6000 microscope captured brightfield and fluorescent images. Leica Application Software Advanced Fluorescence program was used to overlay images to locate nuclei and MWNTs.

To confirm MWNT internalization, TEM images were acquired for RENCA and PC3 cells (3,000 cells in 300-μL solution) following incubation with MWNTs for 2, 4, 6, and 24 hours. Samples were processed with Karnovsky fixative, sectioned into 30 to 50 nm thick slices with a microtome, and placed on copper grids with 200 meshes. Five samples were created from each sample slice. Grids were placed in Petri dishes and stained with 2% uranyl acetate for 12 minutes to increase TEM image contrast. Samples were rinsed with deionized water, dried, and imaged with a transmission electron microscope to determine the number and location of MWNTs within the intracellular space. A voltage of 60 kV was used to prevent sample destruction.

Results

MWNT inclusion enhances light absorption

An absorbance peak is indicative of preferential light absorption and characteristic of heat generation. MWNTs in water exhibited dramatically increased absorption compared with water alone in the wavelength range of 200 to 1,800 nm (shown in Fig. 1). Therefore, significant light absorption and heat generation were anticipated at our target wavelength of 1,064 nm, which was confirmed by measurements of temperature elevation discussed later.

MWNT inclusion increases temperature elevation

For identical heating conditions of 15.3 W/cm^2 for 1.5 minutes, samples containing MWNTs (+NT) produced a significantly greater amount of heat than samples without MWNTs (−NT), with maximum temperature elevations of approximately 30°C and 5°C,

respectively. These temperature elevations for non-MWNT and MWNT samples had standard deviations of 2.10°C and 3.41°C, respectively. When heating duration was increased to 5 minutes, larger temperature elevations were observed for both samples, with elevations of 43°C and 7°C for samples containing and excluding MWNTs, respectively. Temperature elevation for non-MWNT and MWNT samples had standard deviations of 2.25°C and 6.52°C, respectively. The peak temperature elevation and transient temperature response for samples laser heated with and without MWNTs are shown in top and bottom panels of Figure 2, respectively. Six samples were used for each measurement.

MWNTs in combination with laser therapy increase tumor cell death

Figure 3 (top panel) depicts trypan blue staining of PC3 cells (A–C) and RENCA cells (D–F) following inclusion of MWNTs only (A and D), laser heating for 5 minutes without MWNTs (B and E), and laser heating for 5 minutes with MWNTs (C and F). Figure 3 (bottom panel) shows the quantified cell viability for PC3 cells for all conditions. Measured cell viability of PC3 and RENCA cells was nearly identical; therefore, only PC3 quantification is shown. Unheated cells (control) and samples with inclusion of MWNTs showed nearly identical cells viability, validating the nontoxic nature of MWNTs. Cells laser irradiated for 1.5 minutes with and without MWNTs and cells laser treated for 5 minutes maintained high cell viability, similar to untreated samples (−Laser, −NT). However, the combination of laser heating for 5 minutes with MWNTs caused marked differences in cell viability, as evidenced by the extensive trypan blue staining and low cell viability quantification. If MWNTs were not utilized in combination with 15.3 W/cm^2, the irradiance would need to be increased to 50.9 W/cm^2 and the heating duration lengthened to 10 minutes to achieve a similar thermal dose and cell viability.

MWNTs in combination with laser therapy downregulate HSP expression

The expression of HSP27, HSP70, and HSP90 was imaged and quantified for PC3 and RENCA cells with and without MWNT inclusion alone or in combination with laser treatment. Both cell types exhibited similar trends in their HSP expression; therefore, only images and quantified HSP expression for PC3 cells are shown. Figure 4 (top panel) depicts immunofluorescence staining of PC3 cells for the expression of HSP27, HSP70, and HSP90 following several conditions, and Figure 4 (bottom panel) shows the corresponding quantified average mean fluorescence intensity for 3 samples for each HSP. For both cell types, HSP expression was minimal for unheated (control) groups with and without MWNT inclusion (−Laser, −NT and −Laser, +NT), representing the basal HSP expression for PC3 cells. Samples laser treated for 1.5 minutes without MWNTs (15.3 W/cm^2, 1.5 minutes, −NT) experienced increases in HSP expression. Inclusion of MWNTs into the laser treatment protocol (15.3 W/cm^2, 1.5 minutes, +NT) dramatically enhanced HSP expression by increasing the temperature elevation. Because HSP upregulation can increase the likelihood of tumor recurrence, optimizing laser parameters and MWNT concentrations to eliminate HSP expression is critical. Therefore, the heating duration was increased to 5 minutes to cause more substantial temperature elevations to permit downregulation of HSP expression. However, laser irradiation of samples for 5 minutes without MWNT inclusion (15.3 W/cm^2, 5 minutes, −NT) significantly further upregulated the HSP expression. The combination of laser irradiation for 5 minutes with MWNTs (15.3 W/cm^2, 5 minutes, +NT) was required to permit the lethal temperature elevation necessary for downregulating HSP27 and HSP70 expression to basal levels. However, HSP90 levels remained elevated for MWNT-containing samples irradiated at the same heating conditions.

MWNTs undergo cellular uptake

Cellular uptake of MWNTs by PC3 and RENCA cells was imaged with combined brightfield/fluorescence and electron microscopy. Figure 5 (top panel) depicts DAPI-stained

nuclei of RENCA cells overlaid on brightfield images for samples without MWNT inclusion (A and B) and samples containing MWNTs added 24 hours earlier (C and D). Individual MWNTs cannot be visualized because of the diffraction limits of light microscopy; however, MWNT aggregates can be observed as black clusters surrounding the nucleus. MWNTs appear to cross the cell membrane and congregate near the nuclear envelope without being internalized into the nucleus. However, because individual MWNTs cannot be visualized, no conclusions can be drawn regarding whether individual MWNTs cross the nuclear membrane or other cellular organelles. This phenomenon was observed in approximately 40% of the population of both large and small RENCA and PC3 cells.

TEM imaging was used to further investigate the intracellular uptake and distribution of MWNTs within RENCA cells. Figure 5 (bottom panel) depicts the TEM images of intracellular distribution following 2, 4, 6, and 24 hours incubation of MWNTs with cells. After 2 hours of incubation, a significant number of MWNTs were observed within cells, with many aggregating around the nuclear membrane. With increasing incubation periods, larger numbers of MWNTs were observed inside cellular vacuoles and nuclei. Identical intracellular uptake trends were observed in PC3 cells (not shown).

Discussion

This study determined that MWNT inclusion with appropriate laser parameters could dramatically increase temperature elevation, enhance tumor cell destruction, and downregulate HSP expression, thereby providing a potentially more effective and minimally invasive cancer treatment option. The intracellular uptake of MWNTs was also shown and MWNT intracellular distribution was characterized, which provides additional therapeutic opportunities for drug delivery alone or in combination with thermal therapy.

Measuring optical absorption of MWNTs provides a measure of the ability of a sample to absorb light and generate heat due to the composition and geometry of the nanotubes. Optical absorbance measurements indicated that MWNTs possess higher absorption than water in the NIR region (700–1,100 nm), as previously documented (29, 30). This NIR region is clinically relevant due to the extensive penetration depth of light, minimal scattering, and limited heating of superficial tissue layers (26, 29, 30, 43, 44). Absorption of light by MWNTs causes electron excitation followed by nonradiative decay through the vibrational manifold. Because of the high aspect ratio of MWNTs, the electric field within their localized area is enhanced, increasing heat generation (32, 33, 45, 46). Previous work has shown that MWNTs couple with 1,064-nm incident light and generate heat with remarkable efficiency (36, 37, 39). In the present study, the inclusion of MWNTs produced temperature elevations that were drastically higher than MWNT-lacking samples within the same heating regime, demonstrating the heat generation capability of MWNTs.

Inclusion of MWNTs alone (−Laser, +NT) caused no change in cell viability, confirming the lack of inherent toxicity of MWNTs functionalized with pluronic. The inherent toxicity of nanotubes is a long-debated subject due to the many variables affecting their chemical properties and structure. One characteristic that affects toxicity *in vivo* is the surface chemistry of nanotubes. Although pristine nanotubes have very hydrophobic surfaces, surface chemistry modification can render these particles more inert (less toxic) (47, 48). Adding the biocompatible surfactant PL-127 coats the MWNT surface and thus makes the nanotube more biocompatible and water soluble by decreasing nanotube availability to cells and diminishing associated toxicity (36, 37, 40, 41, 49).

Laser irradiation of samples at 15.3 W/cm^2 for 1.5 minutes without MWNT inclusion caused minimal temperature elevation, no significant difference in cell viability, and slight

upregulation of HSP levels, providing a highly ineffective therapy for cancer with a high likelihood of tumor recurrence. Therefore, neither exposure to MWNTs alone nor laser irradiation alone at the chosen parameters caused cell death. Unaided by heat delivery agents such as MWNTs, higher laser irradiances or longer heating durations are required to eradicate tumor cells and prevent HSP upregulation.

Although inclusion of MWNTs enhanced the thermal dose provided by laser irradiation at 15.3 W/cm^2 for 1.5 minutes, tuning of laser parameters is critical to achieving a lethal dose for maximum tumor injury. Laser heating of cells at 15.3 W/cm^2 for 5 minutes without MWNT inclusion significantly enhanced temperature elevation, upregulated HSP expression, and caused no change in cell viability. However, inclusion of MWNTs in this laser therapy yielded dramatically higher temperature elevations, 100% cell death, and down-regulated HSP expression (similar to basal levels). Lengthening the heating time allowed MWNTs to effectively enhance thermal deposition and increase temperatures to lethal limits that resulted in complete cancer cell destruction.

If MWNTs were not utilized in combination with 15.3-W/cm^2 laser heating, the irradiance would need to be increased to 50.9 W/cm^2 [10 W, 5-mm beam diameter (spot size)] and the heating duration lengthened to 10 minutes to achieve a similar thermal dose and cell viability. This clearly illustrates the thermal enhancing capability of MWNTs, substantiating their use as an efficient heat delivery vehicle to treat tissue, as shown in previous work (36, 37, 39).

Significant HSP induction was observed for all HSPs in 3 groups: 1) cells laser treated at 15.3 W/cm^2 for 1.5 minutes without MWNTs; 2) cells laser treated at 15.3 W/cm^2 for 1.5 minutes containing MWNTs; and 3) cells laser treated at 15.3 W/cm^2 for 5 minutes without MWNTs. Elevated HSP expression was expected for all protocols because maximum temperatures achieved were within the HSP upregulation temperature range (44°C–60°C) and lethal thermal dose limits were not exceeded (21, 23, 24). Even though this temperature range is well above the prescribed lethal target temperature used in most therapies (43°C) (31), cells were not heated for an adequate amount of time to effectively damage cells to eliminate HSP expression. However, MWNTs coupled with laser heating at 15.3 W/cm^2 for 5 minutes provided lethal thermal doses causing protein coagulation and a corresponding reduction in expression for both HSP27 and HSP70 to levels similar to basal (control) levels, revealing the destruction of cancer cells before significant induction of HSP began. These data indicate that tuning of laser parameters can produce a therapy that allows control of HSP expression within regions containing MWNTs while preserving viability in regions without MWNTs.

However, HSP90 levels appeared to increase in all treated groups. This discrepancy could be due to the abundance of HSP90 in unstressed cells, accounting for 1% to 2% of all cellular proteins (50). Another explanation involves the temperature activation and destruction of HSP90 compared with the other HSPs. In order for HSP90 to be “activated” so that it can become a fully functional molecular chaperone, oligomerization of HSP90 is required, which is triggered by heat shock (51, 52). Previous research has shown that a rise in intracellular calcium, as witnessed during heat stress, decreases HSP90 thermostability and could account for the ease of HSP90 oligomerization and transition to a fully functional state to perform its molecular chaperone duties (51, 53).

Nanoparticle-induced toxicity is an important area of research (54). Intracellular uptake of nanoparticles is a critical aspect in therapeutic applications such as drug delivery. Developing new strategies for the delivery of therapeutic agents into cells is necessary due to poor cellular penetration of many small molecules and some macromolecules, including

drugs, proteins, and nucleic acids (54, 55). Loading nanoparticles with imaging or therapy moieties could allow for better diagnosis, treatment, and monitoring of disease. Many researchers are investigating the use of nanoparticles as delivery vehicles for therapeutically active molecules (56–58). Our results confirm cellular uptake of MWNTs in both PC3 and RENCA cells. Although brightfield/fluorescence imaging showed MWNT aggregates localized around the nucleus but not inside the nuclear envelope, a more thorough investigation with TEM demonstrated that the rate of cellular uptake and location of MWNTs was dependent on the incubation time. With increasing incubation duration, a greater number of MWNTs were observed in cellular vacuoles and nuclei. The cellular uptake of MWNTs would provide additional advantages for the use of MWNTs in cancer therapy by potentially enhancing other modes of therapy (i.e., reactive oxygen species generation, chemotherapy drug delivery) and imaging methods for diagnosing and monitoring target tissue. Further surface modification will be explored in the future to enhance the capability and rate of cellular uptake.

Acknowledgments

Grant Support

M.N. Rylander: National Science Foundation Grant CBET 0731108, National Institutes of Health (NIH) grant 1 R21 CA135230-01, Virginia Tech Institute for Critical Technology and Applied Science (ICTAS) grant, and Advance Virginia Tech Research Development grant; S.V. Torti: NIH grant RO1CA12842; H.C. Hatcher: Training grant T32CA079448.

References

1. Altekruse, S.; Kosary, C.; Krapcho, M.; Neyman, N.; Aminou, R.; Waldron, W., et al. SEER Cancer Statistics Review, 1975–2007. Bethesda, MD: National Cancer Institute; 2010. [Based on November 2009 SEER data submission]Available from: http://seer.cancer.gov/csr/1975_2007/, http://seer.cancer.gov/statfacts/html/all.html [Accessed August 1, 2010]
2. Amin Z, Bown SG, Lees WR. Local treatment of colorectal liver metastases: a comparison of interstitial laser photocoagulation (ILP) and percutaneous alcohol injection (PAI). Clin Radiol. 1993; 48:166–71. [PubMed: 8403761]
3. Nolsoe CP, Torp-Pedersen S, Burcharth F, Horn T, Pedersen S, Christensen NE, et al. Interstitial hyperthermia of colorectal liver metastases with a US-guided Nd-YAG laser with a diffuser tip: a pilot clinical study. Radiology. 1993; 187:333–7. [PubMed: 8475269]
4. Vogl TJ, Mack MG, Straub R, Engelmann K, Zangos S, Eichler K. Interventional MR-guided laser induced thermotherapy in oncologic indications. Status and prospects. Radiologe. 1999; 39:764–71. [PubMed: 10525634]
5. Seki T, Wakabayashi M, Nakagawa T, Imamura M, Tamai T, Nishimura A, et al. Percutaneous microwave coagulation therapy for patients with small hepatocellular carcinoma: comparison with percutaneous ethanol injection therapy. Cancer. 1999; 85:1694–702. [PubMed: 10223562]
6. Gazelle GS, Goldberg SN, Solbiati L, Livraghi T. Tumor ablation with radio-frequency energy. Radiology. 2000; 217:633–46. [PubMed: 11110923]
7. Hilger I, Andra W, Bahring R, Daum A, Hergt R, Kaiser WA. Evaluation of temperature increase with different amounts of magnetite in liver tissue samples. Invest Radiol. 1997; 32:705–12. [PubMed: 9387059]
8. Hilger I, Hiergeist R, Hergt R, Winnefeld K, Schubert H, Kaiser WA. Thermal ablation of tumors using magnetic nanoparticles: an *in vivo* feasibility study. Invest Radiol. 2002; 37:580–6. [PubMed: 12352168]
9. Jolesz FA, Hynynen K. Magnetic resonance image-guided focused ultrasound surgery. Cancer J. 2002; 8 (Suppl 1):S100–12. [PubMed: 12075696]
10. Madersbacher S, Gröbl M, Kramer G, Dirnhofer S, Steiner GE, Marberger M. Regulation of heat shock protein 27 expression of prostatic cells in response to heat treatment. Prostate. 1998; 37:174–81. [PubMed: 9792134]

11. Gibbons NB, Watson RW, Coffey RN, Brady HP, Fitzpatrick JM. Heat-shock proteins inhibit induction of prostate cancer cell apoptosis. Prostate. 2000; 45:58–65. [PubMed: 10960843]
12. Levine AJ, Momand J, Finlay CA. The p53 tumour suppressor gene. Nature. 1991; 351:453–6. [PubMed: 2046748]
13. Soti C, Nagy E, Giricz Z, Vigh L, Csermely P, Ferdinandy P. Heat shock proteins as emerging therapeutic targets. Br J Pharmacol. 2005; 146:769–80. [PubMed: 16170327]
14. Kiang JG, Tsokos GC. Heat shock protein 70 kDa: molecular biology, biochemistry, and physiology. Pharmacol Ther. 1998; 80:183–201. [PubMed: 9839771]
15. Georgopoulos C, Welch WJ. Role of the major heat shock proteins as molecular chaperones. Annu Rev Cell Biol. 1993; 9:601–34. [PubMed: 8280473]
16. Wiech H, Buchner J, Zimmermann R, Jakob U. Hsp90 chaperones protein folding *in vitro*. Nature. 1992; 358:169–70. [PubMed: 1614549]
17. Tomei, LD.; Cope, FO., editors. Apoptosis: The Molecular Basis of Cell Death. Plainview, NY: Cold Spring Harbor Laboratory Press; 1991.
18. Calderwood SK, Khaleque MA, Sawyer DB, Ciocca DR. Heat shock proteins in cancer: chaperones of tumorigenesis. Trends Biochem Sci. 2006; 31:164–72. [PubMed: 16483782]
19. Ciocca DR, Clark GM, Tandon AK, Fuqua SA, Welch WJ, McGuire WL. Heat shock protein hsp70 in patients with axillary lymph node-negative breast cancer: prognostic implications. J Natl Cancer Inst. 1993; 85:570–4. [PubMed: 8455204]
20. Roigas J, Wallen ES, Loening SA, Moseley PL. Effects of combined treatment of chemotherapeutics and hyperthermia on survival and the regulation of heat shock proteins in Dunning R3327 prostate carcinoma cells. Prostate. 1998; 34:195–202. [PubMed: 9492848]
21. Rylander MN, Diller KR, Wang S, Aggarwal SJ. Correlation of HSP70 expression and cell viability following thermal stimulation of bovine aortic endothelial cells. J Biomech Eng. 2005; 127:751–7. [PubMed: 16248304]
22. Rylander MN, Feng Y, Bass J, Diller KR. Thermally induced injury and heat-shock protein expression in cells and tissues. Ann N Y Acad Sci. 2005; 1066:222–42. [PubMed: 16533928]
23. Rylander MN, Feng Y, Zhang YJ, Stafford JR, Volgin A, Hazle JD, Diller KR. Optimizing heat shock protein expression induced by prostate cancer laser therapy through predictive computational models. J Biomed Opt. 2006; 11:041113–1–16. [PubMed: 16965141]
24. Rylander MN, Feng Y, Bass J, Diller KR. Heat shock protein expression and injury optimization for laser therapy design. Lasers Surg Med. 2007; 39:731–46. [PubMed: 17960756]
25. Wang S, Xie W, Rylander MN, Tucker PW, Aggarwal S, Diller KR. HSP70 kinetics study by continuous observation of HSP-GFP fusion protein expression on a perfusion heating stage. Biotechnol Bioeng. 2007; 99:146–54. [PubMed: 17546686]
26. Kam NW, O'Connell M, Wisdom JA, Dai H. Carbon nanotubes as multifunctional biological transporters and near-infrared agents for selective cancer cell destruction. Proc Natl Acad Sci U S A. 2005; 102:11600–5. [PubMed: 16087878]
27. Bassil A, Puech P, Tubery L, Bacsa W. Controlled laser heating of carbon nanotubes. Appl Phys Lett. 2006; 88:173113–1–3.
28. Poole, CP.; Owens, FJ. Introduction to Nanotechnology. Hoboken, NJ: John Wiley; 2003.
29. Webster, S.; Maultzsch, J.; Thomsen, C.; Liu, J.; Czerw, R.; Terrones, M., et al. Raman Characterization of Nitrogen Doped Multiwalled Carbon Nanotubes. San Francisco, CA: Materials Research Society; 2003. p. 129-34.
30. Xu J, Xiao M, Czerw R, Carroll DL. Optical limiting and enhanced optical nonlinearity in boron-doped carbon nanotubes. Chem Phys Lett. 2004; 389:247–50.
31. Hirsch LR, Stafford RJ, Bankson JA, Sershen SR, Rivera B, Price RE, et al. Nanoshell-mediated near-infrared thermal therapy of tumors under magnetic resonance guidance. Proc Natl Acad Sci U S A. 2003; 100:13549–54. [PubMed: 14597719]
32. Wang Y, Kempa K, Kimball B, et al. Receiving and transmitting light-like radio waves: antenna effect in arrays of aligned carbon nanotubes. Appl Phys Lett. 2004; 85:2607–9.
33. Hanson GW. Fundamental transmitting properties of carbon nanotube antennas. IEEE Trans Antennas Propag. 2005; 53:3426–35.

34. Webster S, Reyes-Reyes M, Pedron X, et al. Enhanced nonlinear transmittance by complementary nonlinear mechanisms: a reverse-saturable absorbing dye blended with nonlinear-scattering carbon nanotubes. Adv Mater. 2005; 17:1239.
35. Dresselhaus MS. Applied physics: nanotube antennas. Nature. 2004; 432:959–60. [PubMed: 15616541]
36. Torti SV, Byrne F, Whelan O, Levi N, Ucer B, Schmid M, et al. Thermal ablation therapeutics based on CN(x) multi-walled nanotubes. Int J Nanomed. 2007; 2:707–14.
37. Burke A, Ding X, Singh R, Kraft RA, Levi-Polyachenko N, Rylander MN, et al. Long-term survival following a single treatment of kidney tumors with multiwalled carbon nanotubes and near-infrared radiation. Proc Natl Acad Sci U S A. 2009; 106:12897–902. [PubMed: 19620717]
38. Liu J, Webster S, Carroll DL. Temperature and flow rate of NH3 effects on nitrogen content and doping environments of carbon nanotubes grown by injection CVD method. J Phys Chem B. 2005; 109:15769–74. [PubMed: 16853001]
39. Sarkar S, Fisher J, Rylander CG, Rylander MN. Photothermal response of tissue phantoms containing multi-walled carbon nano-tubes. J Biomech Eng. 2010; 132:044505–1–5. [PubMed: 20387978]
40. Monteiro-Riviere NA, Inman AO, Wang YY, Nemanich RJ. Surfactant effects on carbon nanotube interactions with human keratinocytes. Nanomedicine. 2005; 1:293–9. [PubMed: 17292102]
41. Moore VC, Strano MS, Haroz EK, Hauge RH, Smalley RE. Individually suspended single-walled carbon nanotubes in various surfactants. Nano Lett. 2003; 3:1379–82.
42. Rylander MN, Feng Y, Zimmermann K, Diller KR. Measurement and mathematical modeling of thermally induced injury and heat shock protein expression kinetics in normal and cancerous prostate cells. Int J Hyperthermia. 2010; 26(8):748–764. [PubMed: 20858083]
43. Schonenberger C, Forro L. Multiwall carbon nanotubes. Phys World. 2000; 13:37–41.
44. Hepplestone SP, Ciavarella AM, Janke C, Srivastava GP. Size and temperature dependence of the specific heat capacity of carbon nanotubes. Surf Sci. 2006; 600:3633–6.
45. Kempa K, Rybczynski J, Huang ZP, Gregorczyk K, Vidan A, Kimball B, et al. Carbon nanotubes as optical antennae. Adv Mater. 2007; 19:421.
46. Burke PJ, Li SD, Yu Z. Quantitative theory of nanowire and nanotube antenna performance. IEEE Trans Nanotechnol. 2006; 5:314–34.
47. Liu Z, Davis C, Cai W, He L, Chen X, Dai H. Circulation and long-term fate of functionalized, biocompatible single-walled carbon nanotubes in mice probed by Raman spectroscopy. Proc Natl Acad Sci U S A. 2008; 105:1410–5. [PubMed: 18230737]
48. Shim M, Kam N, Chen R, Li Y, Dai H. Functionalization of carbon nanotubes for biocompatibility and biomolecular recognition. Nano Lett. 2002; 2:285–8.
49. Matthew JE, Nazario YL, Roberts SC, Bhatia SR. Effect of mammalian cell culture medium on the gelation properties of Pluronic F-127. Biomaterials. 2002; 23:4615–9. [PubMed: 12322983]
50. Csermely P, Schnaider T, Soti C, Prohaszka Z, Nardai G. The 90-kDa molecular chaperone family: structure, function, and clinical applications. A comprehensive review. Pharmacol Ther. 1998; 79:129–68. [PubMed: 9749880]
51. Garnier C, Protasevich I, Gilli R, Tsvetkov P, Lobachov V, Peyrot V, et al. The two-state process of the heat shock protein 90 thermal denaturation: effect of calcium and magnesium. Biochem Biophys Res Commun. 1998; 249:197–201. [PubMed: 9705856]
52. Yonehara M, Minami Y, Kawata Y, Nagai J, Yahara I. Heat-induced chaperone activity of HSP90. J Biol Chem. 1996; 271:2641–5. [PubMed: 8576234]
53. Ding XZ, Smallridge RC, Galloway RJ, Kiang JG. Increases in HSF1 translocation and synthesis in human epidermoid A-431 cells: role of protein kinase C and $[Ca^{2+}]_i$. J Investig Med. 1996; 44:144–53.
54. Unfried K, Albrecht C, Klotz L-O, von Mikecz A, Grether-Beck S, Schins RPF. Cellular responses to nanoparticles: target structures and mechanisms. Nanotoxicology. 2007; 1:52–71.
55. Smith DA, van de Waterbeemd H. Pharmacokinetics and metabolism in early drug discovery. Curr Opin Chem Biol. 1999; 3:373–8. [PubMed: 10419843]

56. Kostarelos K, Lacerda L, Pastorin G, Wu W, Wieckowski S, Luangsivilay J, et al. Cellular uptake of functionalized carbon nanotubes is independent of functional group and cell type. Nat Nanotechnol. 2007; 2:108–13. [PubMed: 18654229]

57. Heller D, Baik S, Eurell T, Strano M. Single-walled carbon nanotube spectroscopy in live cells: towards long-term labels and optical sensors. Adv Mater. 2005; 17:2793–9.

58. Kam NW, Liu Z, Dai H. Carbon nanotubes as intracellular transporters for proteins and DNA: an investigation of the uptake mechanism and pathway. Angew Chem Int Ed Engl. 2006; 45:577–81. [PubMed: 16345107]

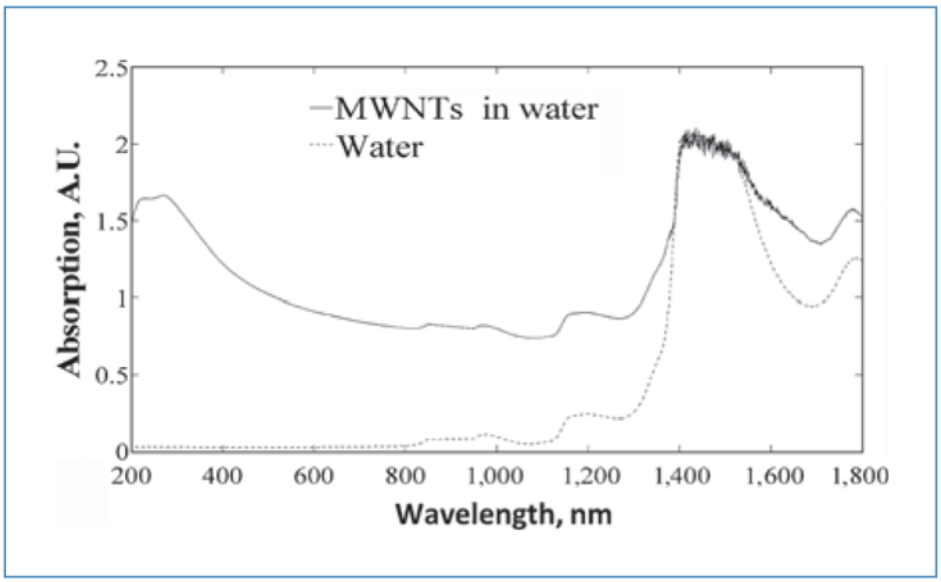

Figure 1.
Absorption spectra for 0.1 mg/mL of MWNTs in deionized water and water alone. Air in a quartz cuvette was used for baseline correction. Scan rate was 600 nm/min.

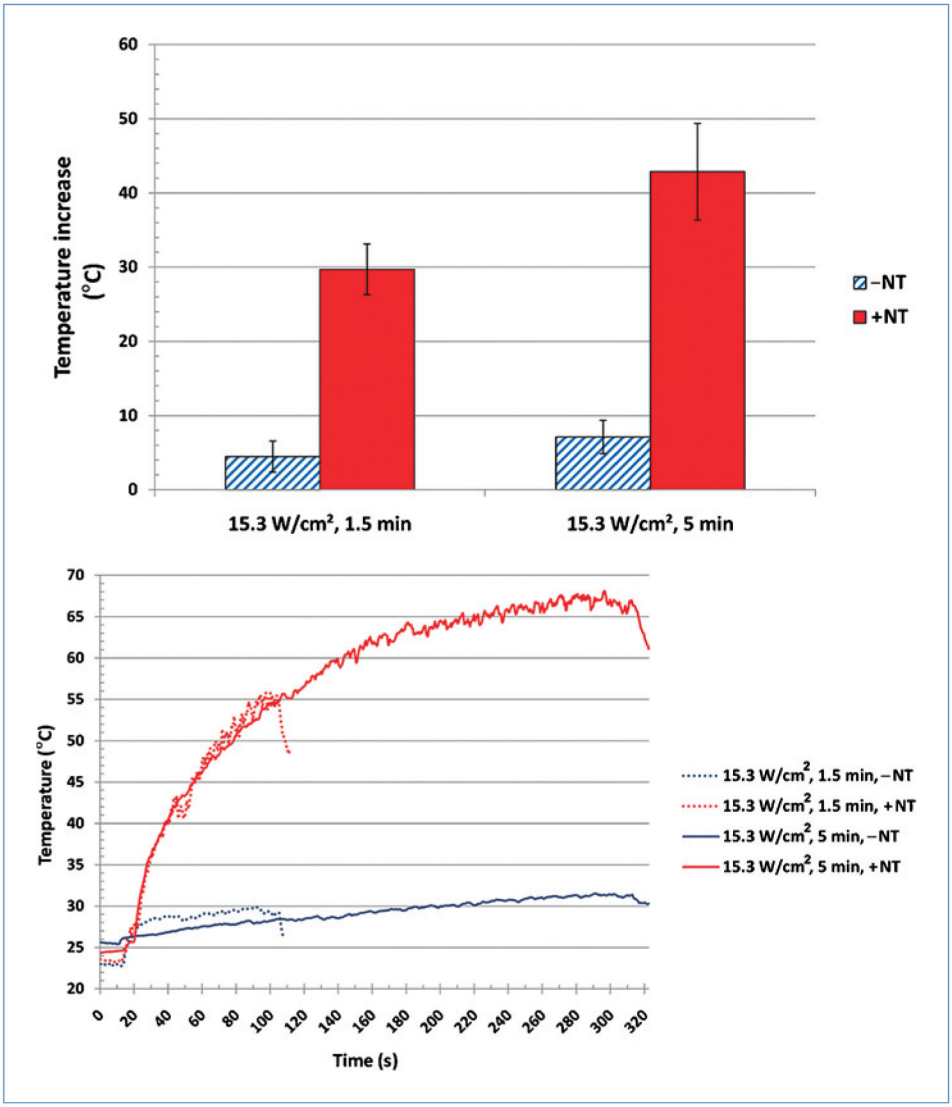

Figure 2.

Top: Temperature elevation following laser heating of media in the absence (−NT) and presence of MWNTs (+NT). *Bottom*: Temperature vs. time plot of laser-heated media in the absence (−NT) and presence of MWNTs (+NT). Both at an irradiance of 15.3 W/cm^2 for 1.5 and 5 min, respectively. Temperatures are measured from a radial distance of 4 mm from the laser center

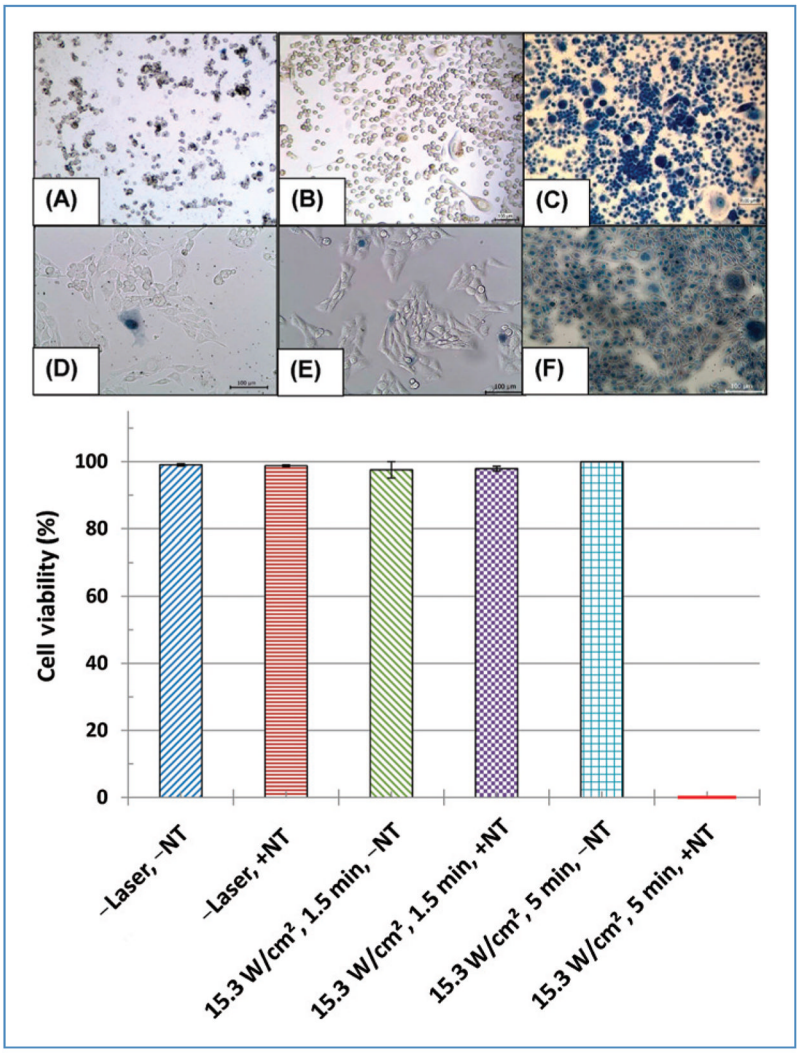

Figure 3.

Top: Trypan blue staining of PC3 cells (A–C) and RENCA cells (D–F) following inclusion of MWNTs only (A, D), laser heating of for 5 min without MWNTs (B, E), and laser heating for 5 min with MWNTs (C, F). Scale bars are 100 μm. *Bottom*: Quantified PC3 cell viability for various treatment protocols.

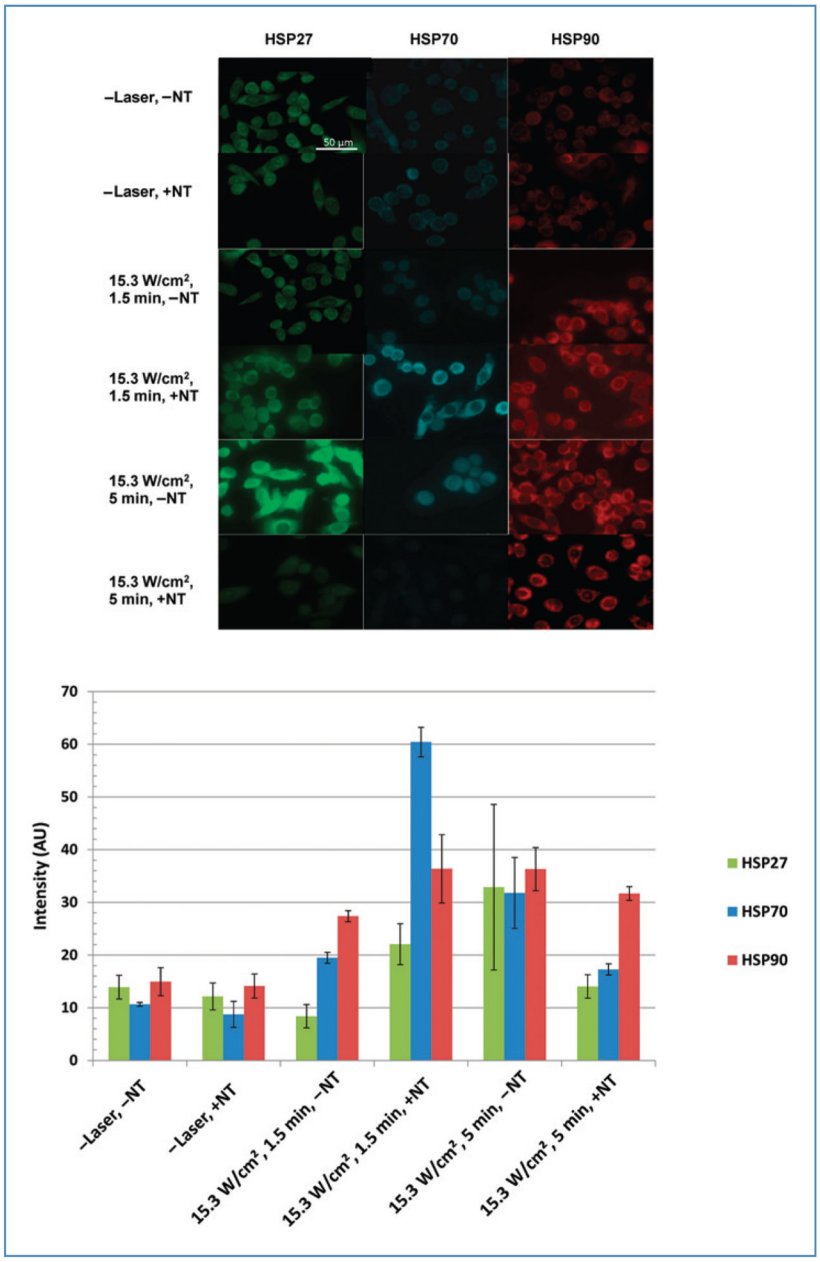

Figure 4.

Top: Fluorescent images of HSP27, 70, and 90 in PC3 cells following various treatment protocols. Scale bars are 50 μm. *Bottom*: Quantified HSP expression for corresponding immunofluorescent images.

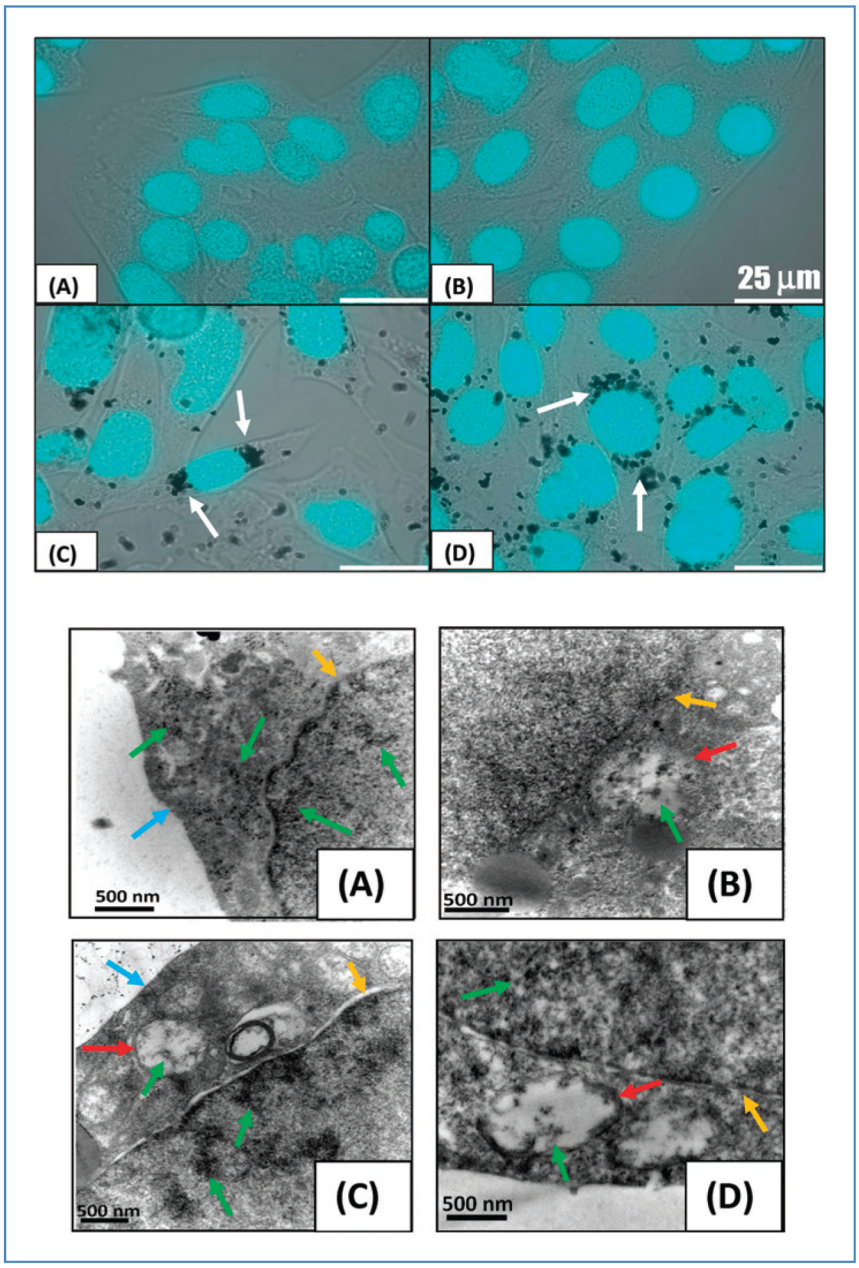

Figure 5.

Top: DAPI-stained nuclei of RENCA cells overlaid on brightfield images. Samples without MWNT inclusion (A, B) and with MWNT added 24 hours earlier (C, D). MWNT aggregates appear as black clusters around the nuclei (see arrows). Scale bars are 25 μm. *Bottom*: TEM images of RENCA cells following MWNT incubation periods of 2 (A), 4 (B), 6 (C), and 24 hours (D). MWNTs were observed inside cell vacuoles (B–D), within nuclear membrane (A–D), and around the nucleus (D), where large aggregate formed. Note arrows indicating cell membrane (blue), nuclear membrane (yellow), vacuoles (red), and MWNT aggregates (green).